ELSEVIER

Journal of Organometallic Chemistry 575 (1999) 223–231

Journal of Organometallic Chemistry

$\{M_3S_2\}$ heterometallic aggregates derived from $Pt_2(PPh_3)_4(\mu\text{-}S)_2$: structural analysis of $[MPt_2X(PPh_3)_5(\mu_3\text{-}S)_2]^+$ (M = Pd and Pt, X = Cl; M = Rh and Ir, X = CO) by X-ray single-crystal crystallography

Zhaohui Li [a], Huang Liu [a], K.F. Mok [a,1], Andrei S. Batsanov [b], Judith A.K. Howard [b], T.S. Andy Hor [a,*]

[a] *Department of Chemistry, Faculty of Science, National University of Singapore, Kent Ridge, Singapore 117600, Singapore*
[b] *Department of Chemistry, University of Durham, Durham DH1 3LE, UK*

Received 4 August 1998; received in revised form 10 September 1998

Abstract

Heterometallic addition of d^8 complexes of Pd(II), Pt(II), Rh(I) and Ir(I) to $Pt_2(PPh_3)_4(\mu\text{-}S)_2$ results in triangular aggregates $[MPt_2X(PPh_3)_5(\mu_3\text{-}S)_2]^+$ (M = Pd and Pt, X = Cl; M = Rh and Ir, X = CO) characterized by ^{31}P-NMR spectroscopy and X-ray single-crystal crystallography. They show a trigonal bipyramidal $\{MPt_2S_2\}$ core with three d^8 sq-planar metal atoms aligned at close proximity but without direct M–M bonds. Unlike their d^{10} counterparts [Ag(I) and Cu(I)], these aggregates resist desulfurization under ambient pressure of CO.

Keywords: Heterometallic; Triangular; Aggregate; Carbon monoxide; Platinum; Sulfide; X-ray single-crystal crystallography

1. Introduction

The use of $Pt_2(PPh_3)_4(\mu\text{-}S)_2$, **1**, as a synthon for the synthesis of $\{M_3S_2\}$ and $\{M_4S_2\}$ aggregates has been established [1–6]. The ability for **1** to capture a variety of metal fragments makes it one of the most useful precursors for heterometallic work [1–5,7,8]. The versatility of the synthesis is traced to the facility of the Lewis acid/base addition [9–13]. Recently, this strategy has been extended to cluster synthesis taking advantage of the desulfurization property of gaseous CO [14]. In this paper, we shall describe the interaction of **1** with four typical d^8 metals, Pd(II), Pt(II), Ir(I) and Rh(I), under a CO atmosphere. Triangular clusters and aggregates comprising solely d^8 metal centers are of interest because of their ability to give a range of positional isomers. The study of these isomers is often a subject of substantial structural and catalytic interest [5,9].

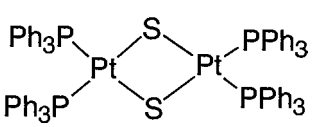

(**1**)

2. Results and discussion

An equimolar mixture of **1** and $PdCl_2(PPh_3)_2$ under a mild CO atmosphere (60 psi) in an autoclave at 80°C does not lead to any desulfurization or carbonyl complexes. Metathesis of the product with NH_4PF_6 gives a complex analyzed as $[PdPt_2Cl(PPh_3)_5(\mu_3\text{-}S)_2]PF_6$, **2** (Fig. 1). We initially assigned this as the same complex as that obtained from the bridge-cleavage reaction of

* Corresponding author. Fax: +65-779-1691; e-mail: chmandyh@nus.edu.sg.
[1] Also corresponding author.

0022-328X/99/$ - see front matter
PII: S0022-328X(98)00998-X

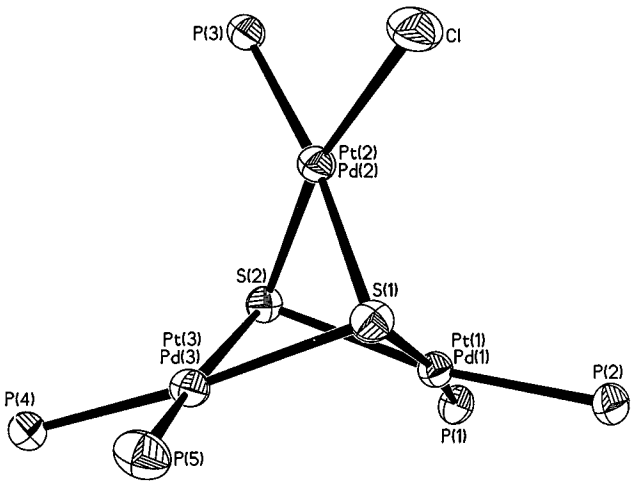

Fig. 1. ORTEP plot of the molecular structure of $[M_3Cl(PPh_3)5(\mu_3\text{-}S)_2]^+$ ($M_3 = Pd_{1.1}Pt_{1.9}$), **2** with 50% probability thermal ellipsoids (phenyl rings removed for clarity).

$[Pd_2Pt_4(PPh_3)_8(\mu\text{-}Cl)_2(\mu\text{-}S)_4]^{2+}$ by PPh_3 [7]. However, the ^{31}P-NMR spectrum of **2** is significantly more complex than the expected A_2B_2X pattern. Although a complete analysis is currently not possible, the spectrum of the analytically pure product appears to suggest a mixture of isomers of similar structural characteristics. We therefore carried out a single-crystal X-ray crystallographic analysis on **2**. It shows a sulfide-bicapped M_3 core with two metals bearing two PPh_3 groups and the remaining one carrying a chloride and a PPh_3 ligand (Fig. 1). The presence of an uncoordinated PF_6^- is agreeable to the d^8 formulation of all the three metals which in turn is consistent with the sq-planar geometry of the metals without significant M–M overlaps. Identification of the metals however presents an interesting chemical and crystallographic problem. Although the synthetic design is targeted at a $\{PdPt_2\}$ core with chloride on Pd, it is equally possible, chemically and structurally, to have a $\{Pd_2Pt\}$ core or a $\{PdPt_2\}$ core with chloride on either of the Pt centers. This is the inherent characteristic of a triangular aggregate containing only d^8 metals. This form of positional isomerism is envisaged upon metal interchange through a $\{M_3S_2\}$ core (Scheme 1) or chloride–phosphine exchange between two neighboring heterometals (Scheme 2). The present crystallographic analysis suggests that the Pt and Pd atoms are statistically disordered; a refinement of the occupancies of the three metal atoms indicates M(1) to be 0.8Pt + 0.2Pd, M(2) to be 0.6Pd + 0.4Pt and M(3) to be 0.7Pt + 0.3Pd. The formula is hence strictly represented as $[Pd_{1.1}Pt_{1.9}Cl(PPh_3)_5(\mu_3\text{-}S)_2]PF_6{\cdot}H_2O$, the complex therefore represents a statistical mixture of the $\{PdPt_2\}$ and $\{Pd_2Pt\}$ isomers. The uneven distribution of different metal residues on the M_3 core is reflected in some structural distortions of the M_3 core. These are represented by some uneven M···M separations (3.067(2), 3.133(2) and 3.294(2) Å) which are intermediate between the Pt···Pt (3.367(2) Å) and Pt···Pd (3.005(2) Å) separations in $[Pd_2Pt_4(PPh_3)_8(\mu\text{-}Cl)_2(\mu_3\text{-}S)_4][PF_6]_2$ and larger than the Pd···Pd separations in $[Pd_3Cl(dppf)_2(PPh_3)(\mu_3\text{-}S)_2]^+$ (3.0867(8), 3.0923(8) and 3.2383(8) Å) [15]. These variations arise from the uneven metal distributions and structural asymmetry of the core. The M–S lengths accordingly span over a wide range of 2.318(1)–2.385(1) Å. The M–S–M angles also differ significantly within each half of the tbp structure (81.65(4)–89.00(4)° and 81.40(4)–88.22(4)°) (Tables 1 and 2).

When **1** and $PtCl_2(PPh_3)_2$ are similarly mixed in an autoclave in a CO atmosphere, a Pt_3^{II} aggregate, $[Pt_3Cl(PPh_3)_5(\mu_3\text{-}S)_2]Cl$, **3a**, results. It is noteworthy that there is no evidence for the formation of other positional isomers such as $Pt_3Cl_2(PPh_3)_4(\mu_3\text{-}S)_2$ or $[Pt_3(PPh_3)_6(\mu_3\text{-}S)_2]Cl_2$, although both have been reported [6]. The absence of any chloride or phosphine exchange isomers is understood based on the lower lability of the Pt–P and Pt–Cl bonds. The ^{31}P-NMR spectrum displays three distinct resonances (δ 14.8, 12.9 and 8.9 ppm) in a 2:2:1 intensity ratio. This is consistent with five PPh_3 ligands on three metals with two ligands above the metal plane, two below, and one on the distinct Pt site that carries a chloride. The solid-

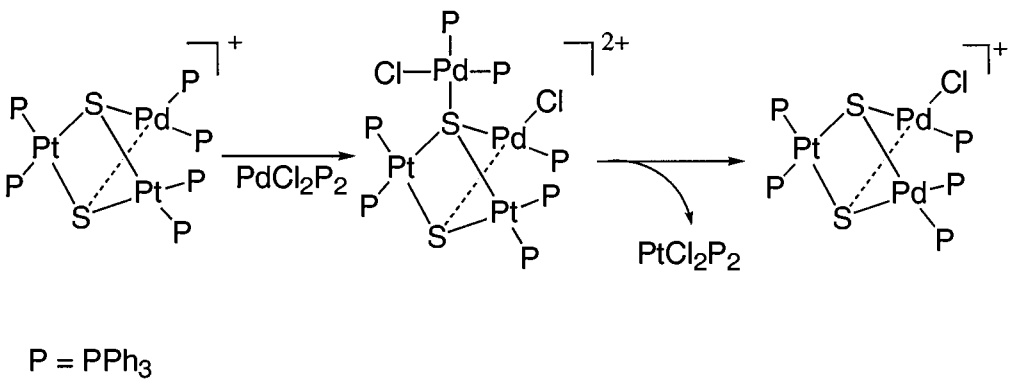

Scheme 1. Metal interchange through a $\{M_4S_2\}$ core.

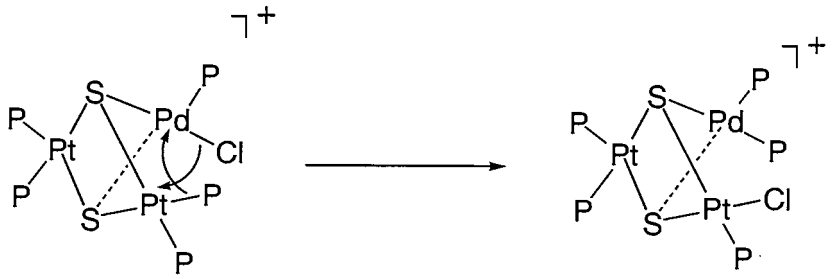

Scheme 2. Chloride–phosphine exchange between two neighboring heterometals.

state structure of the PF_6^- salt **3b** (Fig. 2) shows an isosceles platinum triangle capped by sulfide on either side of the metal plane. The Pt···Pt separation between the $[Pt(PPh_3)_2]$ moieties (3.301(2) Å) is significantly higher than the other two distances involving the sterically less demanding $[PtCl(PPh_3)]$ fragment (3.088(1) and 3.134(1) Å). This contrasts that in $[Pt_3(dppe)_3(\mu_3\text{-}S)_2]^{2+}$ [16], which shows three nearly identical Pt···Pt separations (3.132(3), 3.093(3) and 3.140(3) Å) because of the C_3 symmetry. The molecular asymmetry of **3** is also reflected in the significant variations in the Pt–S distances (2.338(5)–2.384(5) Å) and Pt–S–Pt angles (81.4(2)–89.1(2)°). The steric effect associated with the $[Pt(PPh_3)_2]$ moieties is further supported by the large Pt–S–Pt angles associated with it (88.7(2) and 89.1(2)°). The average Pt–S distance of 2.354(5) Å is marginally larger than the M–S length in **2** (2.344(1) Å). This is expected based on the similarities of **2** and **3**.

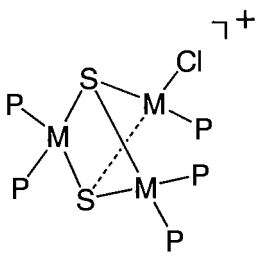

M = Pd, Pt (**2**)

M = Pt (**3**)

P = PPh_3

Similar reaction of **1** with $RhCl(CO)(PPh_3)_2$ under 60 psi CO pressure in THF gives $[Pt_2Rh(CO)(PPh_3)_5(\mu_3\text{-}S)_2]Cl$, **4a** ($\nu_{CO}$ 1964 cm^{-1}) and an unidentified platinum compound. Changing the solvent to methanol and using a higher CO pressure (80 psi) leads to almost pure complex **4a**. Use of $RhCl_3{\cdot}3H_2O$ or other Rh(I) precursors such as $RhHCO(PPh_3)_3$ and $RhCl(PPh_3)_3$ gives the same product. Complex **4a** slowly decomposes in solution but is significantly more stable in the solid state. Two discrete resonance in the $^{31}P\{^1H\}$ spectrum suggests two sets of inequivalent phosphines on Pt (δ 18.4, 15.8 ppm) which is a consequence of two different terminal ligands on the Rh(I) center. X-ray analysis of its PF_6^- salt, **4b**, shows a $\{RhPt_2S_2\}$ tbp core with a carbonyl group on Rh(I) and the remaining sites filled by PPh_3 (Fig. 3). The Pt···Rh separation (3.078(1) Å av.) is significantly shorter than the Pt···Pt separation (3.312(5) Å) for steric reasons. Accordingly, the Pt–S–Pt angles (89.49(4)° av.) are significantly greater than the Pt–S–Rh ones (81.26(4)° av.). The metal moieties are geometrically confined to close proximity by the sulfide ligands, giving short non-bonding Pt···Rh contacts which could be compared with some longer Pt–Rh bonds, e.g. 2.698(2)–3.167(2) Å in $[PtRh_6(CO)_{16}]^{2-}$ [17]. The lack of direct Rh–Pt bond is supported by the lack of coupling between the phosphines on the different metals. The Rh–S bonds (2.375(1) Å av.) are longer than the Pt–S (2.352(1) Å av.) ones due to the higher electrostatic attractions of Pt(II) compared to Rh(I) with sulfide.

Reaction of **1** with $IrHCO(PPh_3)_3$ under similar conditions as in **4a** gives $[IrPt_2(CO)(PPh_3)_5(\mu\text{-}S)_2]Cl$, **5a** ($\nu_{CO}$ 1954 cm^{-1}) which is isomorphous to **4a**. Similarly, **5a** is unstable in solution but more stable in the solid state. The $^{31}P\{^1H\}$ spectrum shows an Ir-bonded PPh_3 at δ 15.8 ppm and the Pt-bonded PPh_3 at δ 15.2 and 11.9 ppm. X-ray diffraction study of its PF_6^- salt, **5b** (Fig. 4), also shows a $\{IrPt_2S_2\}$ tbp with one carbonyl and one PPh_3 group on Ir(I). The Ir···Pt distance (3.092 (1) Å av.) is much longer than the carbonyl-bridged Ir–Pt bonds (2.701(4)–2.709(5) Å) but comparable to the unbridged Ir–Pt bonds (3.024(4) Å) in $[PtIr_4(CO)_9(\mu\text{-}CO)_5]^{2-}$ [18]. The Pt···Ir separation (3.092(1) Å av.) is significantly shorter than the Pt···Pt separation (3.315(5) Å) because of the four bulky PPh_3 ligands on platinum. These non-bonding metal separations are comparable to those in **4b**. The Pt–S–Pt angles (89.15(5)° av.) are accordingly significantly greater than those of Pt–S–Ir (81.53(5)° av.). The Ir–S bonds (2.375(2) Å av.) are essentially the same as the Rh–S bonds (2.375(1) Å av.) in **4b**, which is not unexpected in view of the similarity of Ir(I) and Rh(I) and between **4b** and **5b**.

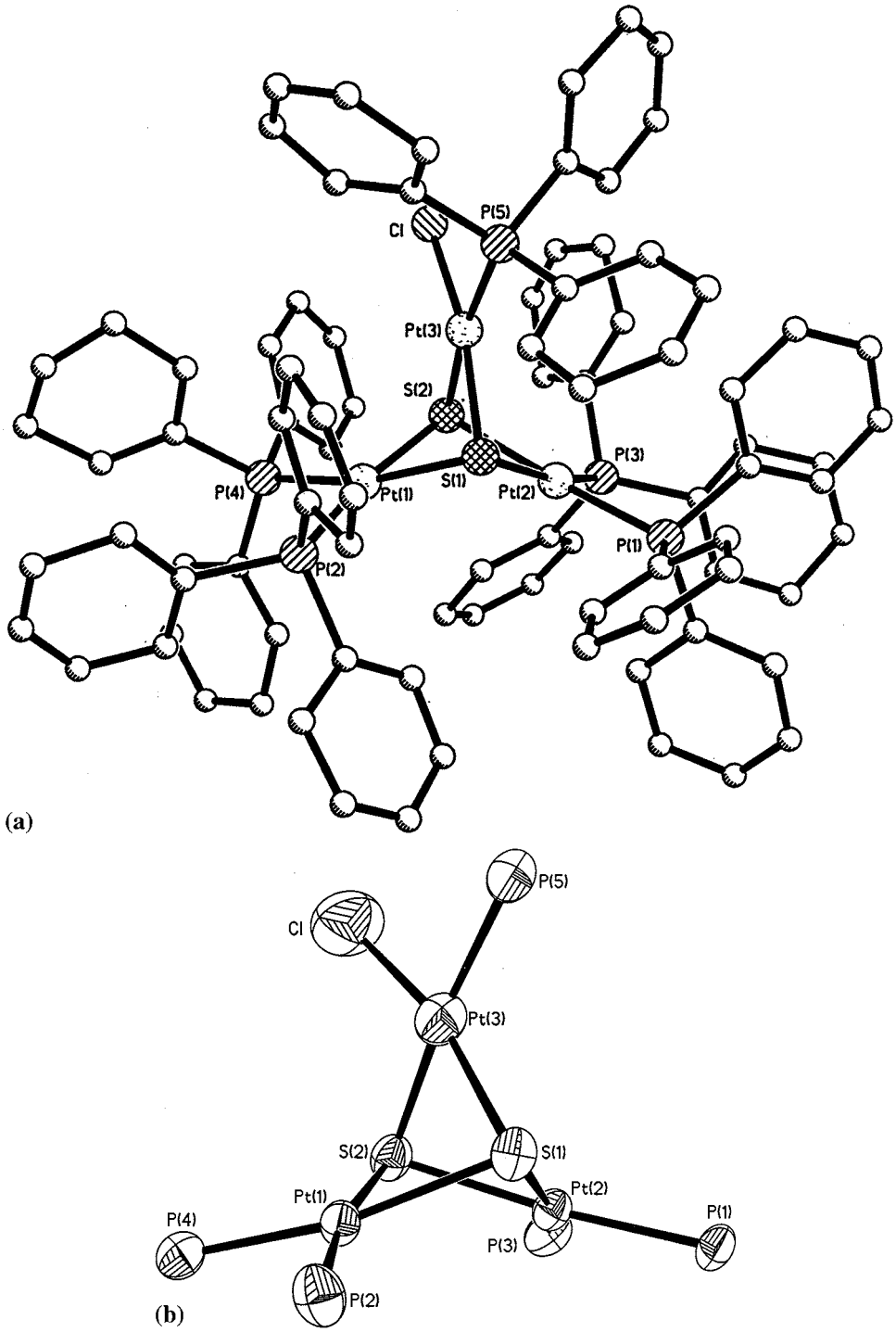

Fig. 2. ORTEP plot of the molecular structure of $[Pt_3Cl(PPh_3)_5(\mu_3\text{-}S)_2]^+$, **3b** with 50% probability thermal ellipsoids (a) with phenyl rings and (b) phenyl rings removed for clarity.

Although similar reactions of **1** with the d^{10} metals lead to partial desulfurization resulting in cluster compounds, no such products are apparent in these reactions with the d^8 metals. We attribute this to the strength of the M–S bonds and the high stability of the tbp M_3S_2 core when made up of d^8 metals. Desulfurization by CO occurs in the form of elimination of COS which could occur by an intramolecular elimination mechanism via the formation of a carbonyl complex with bridging sulfide, viz. $(OC)M(\mu\text{-}S)M \rightarrow M\text{–}M + COS$ [19]. The lack of affinity of Pt(II)/Pd(II) metals for carbonyl ligands and the higher stability of Rh(I) and Ir(I) carbonyl complexes could also make it difficult for such COS elimination to occur. These factors account

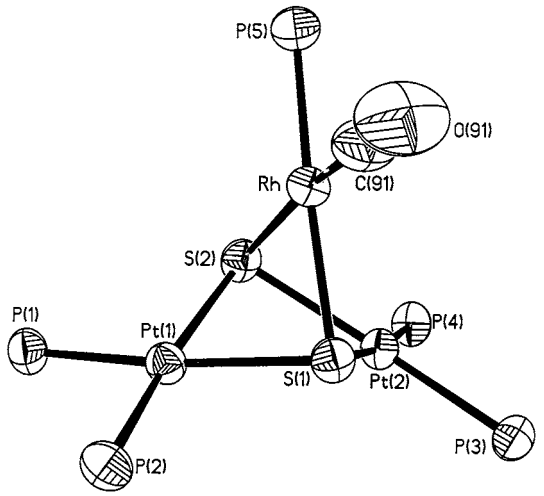

Fig. 3. ORTEP plot of the molecular structure of $[Pt_2Rh(CO)(PPh_3)_5(\mu_3\text{-}S)_2]^+$, **4b** with 50% probability thermal ellipsoids (phenyl rings and solvate removed for clarity).

for the higher resistance of these complexes towards desulfurization to give clusters. We are in the process of studying the interactions of **4** and **5** with CO under more forcing conditions.

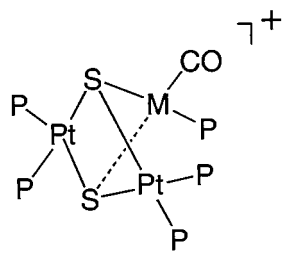

M = Rh (**4**) , Ir (**5**)

P = PPh_3

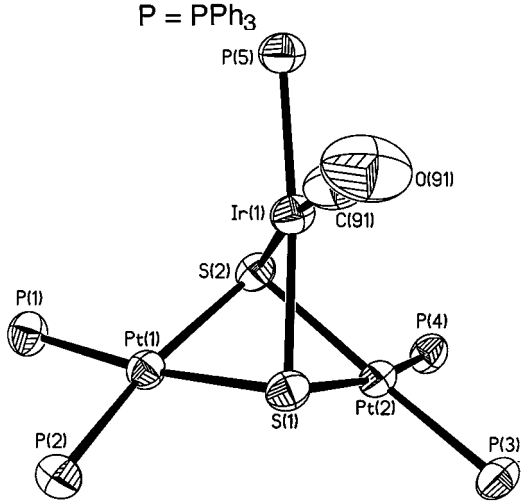

Fig. 4. ORTEP plot of the molecular structure of $[Pt_2Ir(CO)(PPh_3)_5(\mu_3\text{-}S)_2]^+$, **5b** with 50% probability thermal ellipsoids (phenyl rings and solvate removed for clarity).

3. Experimental details

3.1. General

All solvents were distiled and deoxygenated by argon before use. Complex **1** was synthesized from $PtCl_2(PPh_3)_2$ and $Na_2S{\cdot}2H_2O$ according to the literature method [20]. $RhClCO(PPh_3)_2$ [21], $RhCl(PPh_3)_3$ [21] and $RhHCO(PPh_3)_3$ [22] were synthesized from $RhCl_3{\cdot}3H_2O$. Other chemicals were used as supplied. Elemental analyses were carried out in the Microanalytical Laboratory in the Chemistry Department of the National University of Singapore (NUS). Infra-red spectra were taken in KBr disc on a Perkin Elmer 1600 FT–IR spectrophotometer. Solution conductivity measurements were measured by using a STEM conductivity 1000 m with cell constant 0.65 cm^{-1}. $^{31}P\{^1H\}$-NMR spectra were run on a Bruker ACF 300 spectrometer.

3.2. Synthesis of $[M_3Cl(PPh_3)_5(\mu_3\text{-}S)_2]PF_6$ ($M_3 = Pd_{1.1}Pt_{1.9}$), **2**

A suspension of complex **1** (0.15 g, 0.1 mmol) and $PdCl_2(PPh_3)_3$ (0.070 g, 0.1 mmol) in THF (40 cm^3) was flushed with CO and stirred in an autoclave at 80°C under a CO pressure of 60 psi. After 24 h a clear orange solution was obtained. The resultant solution was filtered and the filtrate was concentrated to ca. 15 cm^3 under vacuum. Hexane (70 cm^3) was added to give rise to an orange precipitate. Molar conductivity Λ_m (10^{-3} M, MeOH): 96 $cm^2\ \Omega^{-1}\ mol^{-1}$. The product was further purified by a metathesis reaction with NH_4PF_6 to yield $[Pd_{1.1}Pt_{1.9}Cl(PPh_3)_5(\mu_3\text{-}S)_2]PF_6$ **2**. (0.133 g, 65%). Anal. Calc. for $C_{90}H_{75}F_6ClP_6Pd_{1.1}Pt_{1.9}S_2$: C, 52.9; H, 3.7; Cl, 1.7; P, 9.1; Pd, 5.7; Pt, 18.2; S, 3.1%. Found: C, 51.3; H, 3.2; Cl, 1.9; P, 8.6; Pd, 5.3; Pt, 17.1; S, 2.8%. IR (cm^{-1}) 839 vs (PF_6^{-1}). The presence of isomers in solution gives a complex $^{31}P\{^1H\}$-NMR spectrum, but the major peaks are at 19.4 (m), 17.4 (m) and 16.1 (m).

3.3. Synthesis of $[Pt_3Cl(PPh_3)_5(\mu_3\text{-}S)_2]PF_6$, **3b**

Complex **3** was synthesized in a manner analogous to **2** by using **1** (0.15 g, 0.1 mmol) and $PtCl_2(PPh_3)_2$ (0.079 g, 0.1 mmol) in THF (40 cm^3). The suspension was flushed with CO and stirred in an autoclave at 80°C under a CO pressure of 60 psi. After 24 h a clear orange solution was obtained. The resultant solution was filtered and the filtrate was concentrated to ca. 15 cm^3 under vacuum. Hexane (70 cm^3) was added to give rise to an orange precipitate which was further purified by recrystallization from CH_2Cl_2/hexane to isolate $[Pt_3Cl(PPh_3)_5(\mu_3\text{-}S)_2]Cl$, **3a** (Yield 0.085 g, 42%). Molar conductivity Λ_m (10^{-3} M, MeOH): 92 $cm^2\ \Omega^{-1}\ mol^{-1}$. **3a** reacts with excess NH_4PF_6 in MeOH to yield $[Pt_3Cl(PPh_3)_5(\mu_3\text{-}S)_2]PF_6$, **3b**. Anal. Calc. for

Table 1
Crystallographic data and refinement details for $[M_3Cl(PPh_3)_5(\mu_3\text{-}S)_2]PF_6\cdot H_2O$ ($M = Pd_{1.1}Pt_{1.9}$), **2**; $[Pt_3Cl(PPh_3)_5(\mu_3\text{-}S)_2]PF_6$, **3b**; $[RhPt_2(CO)(PPh_3)_5(\mu_3\text{-}S)_2]PF_6\cdot CH_2Cl_2$, **4b**, and $[IrPt_2(CO)(PPh_3)_5(\mu_3\text{-}S)_2]PF_6\cdot\frac{1}{2}CH_2Cl_2$, **5b**

	2	**3b**	**4b**	**5b**
Chemical formula	$C_{90}H_{77}ClF_6OP_6Pd_{1.1}Pt_{1.9}S_2$	$C_{90}H_{75}ClF_6P_6Pt_3S_2$	$C_{92}H_{77}Cl_2F_6OP_6Pt_2RhS_2$	$C_{91.5}H_{76}Cl_1F_6OP_6Pt_2IrS_2$
Formula weight	2064.9	2141.2	2126.5	2173.3
Crystal size (mm)	$0.25\times0.30\times0.45$	$0.15\times0.18\times0.40$	$0.40\times0.31\times0.15$	$0.70\times0.51\times0.40$
Crystal system	Orthorhombic	Orthorhombic	Orthorhombic	Orthorhombic
Space group	*Pbca*	*Pbca*	*Pbca*	*Pbca*
a (Å)	24.046(3)	24.226(5)	24.401(8)	24.421(5)
b (Å)	25.411(3)	25.506(5)	25.817(6)	25.879(2)
c (Å)	27.300(3)	27.556(6)	27.675(4)	27.683(2)
V (Å^3)	16 681(3)	17 027(6)	17 434(7)	17 496(1)
Z	8	8	8	8
$D_{calc.}$ (g cm^{-3})	1.644	1.671	1.620	1.650
μ (mm^{-1})	3.726	5.168	3.667	4.954
$F(000)$	8144	8336	8384	8472
θ range for data collection (°)	1.38–30.81	1.37–23.05	1.58–26.49	1.57–26.48
hkl range	0–33, 0–36 and 0–38	0–26, 0–28 and 0–30	−27–30, −32–31 and −34–21	−30–19, −32–30 and −34–34
Number of reflections collected	24 118	10 306	95 659	91 412
Number of unique data	23 685	10 306	17 965	17 903
Number of reflections [$I>2\sigma(I)$]	16 916	5892	13 785	13 888
Min/max transmission	0.518, 0.740	0.709, 0.972	0.607, 0.928	0.475, 0.928
Number of variables	985	973	1009	1009
Residuals: R_1[a], wR_2[b] (obs. data)[a]	0.0451, 0.0692	0.0655, 0.1712	0.0439, 0.0678	0.0440, 0.1026
Residuals: R_1[a], wR_2[b] (all data)[a]	0.0915, 0.1055	0.1310, 0.1783	0.0689, 0.0758	0.0668, 0.1138
Weighting scheme, w^{-1}	$\sigma^2(F_o)^2+70.53\rho$	$\sigma^2(F_o)^2+(0.0926\rho)^2$	$\sigma^2(F_o)^2+(0.0107\rho)^2+44.53\rho$	$\sigma^2(F_o)^2+(0.0446\rho)^2+58.21\rho$
Goodness of fit	1.30	0.932	1.151	1.133
$(\Delta\rho)_{max}$, $(\Delta\rho)_{min}$ (e Å^{-3})	1.752, −0.991	3.52, −2.69	0.857, −0.823	1.636, −1.393

[a] $R_1 = \Sigma\big||F_o|-|F_c|\big|/\Sigma|F_o|$.
[b] $wR_2 = \{\Sigma w[(F_o^2-F_c^2)^2]/\Sigma wF_o^4\}^{1/2}$; $\rho = [\max(F_o^2,\theta)+2F_c^2]/3$.

Table 2
Selected bond lengths (Å), angles (°) for **2**, **3b**, **4b** and **5b**

(a) $[M_3Cl(PPh_3)_5(\mu_3\text{-}S)_2]PF_6\cdot H_2O$ ($M = Pd_{1.1}Pt_{1.9}$), ***2***[a]			
M(1)–S(1)	2.336(1)	M(1)–S(2)	2.385(1)
M(1)–P(1)	2.290(1)	M(1)–P(2)	2.285(1)
M(2)–S(1)	2.318(1)	M(2)–S(2)	2.318(1)
M(2)–P(3)	2.270(1)	M(2)–Cl	2.369(1)
M(3)–S(1)	2.364(1)	M(3)–S(2)	2.347(1)
M(3)–P(4)	2.295(1)	M(3)–P(5)	2.300(2)
M(1)···M(2)	3.067(2)	M(3)···M(2)	3.133(2)
M(1)···M(3)	3.294(2)		
M(1)–S(1)–M(3)	89.00(4)	M(1)–S(2)–(3)	88.22(4)
M(1)–S(1)–M(2)	81.65(4)	M(1)–S(2)–(2)	81.40(4)
M(3)–S(1)–M(2)	83.18(4)	M(3)–S(2)–(2)	84.40(4)
S(1)–M(1)–S(2)	77.46(4)	S(1)–M(1)–P(1)	168.88(5)
S(1)–M(1)–P(2)	91.64(5)	S(2)–M(1)–P(1)	91.67(5)
S(2)–M(1)–P(2)	166.46(5)	P(1)–M(1)–P(2)	99.45(5)
S(1)–M(2)–S(2)	78.39(4)	S(1)–M(2)–P(3)	172.26(5)
S(1)–M(2)–Cl	90.89	S(2)–M(2)–P(3)	99.77(5)
S(2)–M(2)–Cl	166.49(5)	P(3)–M(2)–Cl	91.94(5)
S(1)–M(3)–S(2)	77.67(4)	S(1)–M(3)–P(4)	172.84(5)
S(1)–M(3)–P(5)	87.11(5)	S(2)–M(3)–P(4)	95.90(5)
S(2)–M(3)–P(5)	163.97(5)	P(4)–M(3)–P(5)	99.00(5)
(b) $[Pt_3Cl(PPh_3)_5(\mu_3\text{-}S)_2]PF_6$, ***3b***			
Pt(1)–S(1)	2.384(5)	Pt(1)–S(2)	2.347(5)
Pt(1)–P(2)	2.275(5)	Pt(1)–P(4)	2.278(6)
Pt(2)–S(1)	2.338(5)	Pt(2)–S(2)	2.357(5)
Pt(2)–P(1)	2.287(5)	Pt(2)–P(3)	2.299(6)
Pt(3)–S(1)	2.350(5)	Pt(3)–S(2)	2.349(5)
Pt(3)–P(5)	2.229(6)	Pt(3)–Cl	2.388(7)
Pt(1)···Pt(3)	3.088(1)	Pt(2)···Pt(3)	3.134(1)
Pt(1)···Pt(2)	3.301(2)		
Pt(1)–S(1)–Pt(2)	88.7(2)	Pt(1)–S(2)–Pt(2)	89.1(2)
Pt(1)–S(1)–Pt(3)	81.4(2)	Pt(1)–S(2)–Pt(3)	82.0(2)
Pt(2)–S(1)–Pt(3)	83.9(2)	Pt(2)–S(2)–Pt(3)	83.5(2)
S(1)–Pt(1)–S(2)	77.2(2)	S(1)–Pt(1)–P(2)	91.4(2)
S(1)–Pt(1)–P(4)	166.8(2)	S(2)–Pt(1)–P(2)	168.3(2)
S(2)–Pt(1)–P(4)	91.9(2)	P(2)–Pt(1)–P(4)	99.8(2)
S(1)–Pt(2)–S(2)	77.9(2)	S(1)–Pt(2)–P(1)	95.7(2)
S(1)–Pt(2)–P(3)	164.0(2)	S(2)–Pt(2)–P(1)	172.6(2)
S(2)–Pt(2)–P(3)	86.7(2)	P(1)–Pt(2)–P(3)	99.3(2)
S(1)–Pt(3)–S(2)	77.8(2)	S(1)–Pt(3)–P(5)	101.6(2)
S(1)–Pt(3)–Cl	166.9(2)	S(2)–Pt(3)–P(5)	172.7(2)
S(2)–Pt(3)–Cl	90.7(2)	P(5)–Pt(3)–Cl	90.6(2)
(c) $[RhPt_2(CO)(PPh_3)_5(\mu_3\text{-}S)_2]PF_6\cdot CH_2Cl_2$, ***4b***			
Pt(1)–P(1)	2.2850(14)	Pt(1)–P(2)	2.2765(14)
Pt(1)–S(1)	2.3304(14)	Pt(1)–S(2)	2.3723(13)
Pt(2)–P(3)	2.296(2)	Pt(2)–P(4)	2.2819(14)
Pt(2)–S(1)	2.3542(13)	Pt(2)–S(2)	2.3528(14)
Rh–C(91)	1.867(7)	Rh–P(5)	2.261(2)
Rh–S(1)	2.3619(14)	Rh–S(2)	2.3887(14)
C(91)–O(91)	1.099(7)		
Pt(1)···Rh	3.0658(10)	Pt(2)···Rh	3.0908(6)
Pt(1)···Pt(2)	3.312(5)		
P(1)–Pt(1)–P(2)	100.00(5)	P(1)–Pt(1)–S(1)	168.29(5)
P(1)–Pt(1)–S(2)	89.66(5)	P(2)–Pt(1)–S(1)	91.63(5)
P(2)–Pt(1)–S(2)	169.17(5)	S(1)–Pt(1)–S(2)	78.88(4)
P(3)–Pt(2)–P(4)	98.82(5)	P(3)–Pt(2)–S(1)	86.44(5)
P(3)–Pt(2)–S(2)	165.09(5)	P(4)–Pt(2)–S(1)	173.39(5)
P(4)–Pt(2)–S(2)	95.76(5)	S(1)–Pt(2)–S(2)	78.80(4)
C(91)–Rh–P(5)	91.1(2)	C(91)–Rh–S(1)	91.8(2)
C(91)–Rh–S(2)	169.0(2)	P(5)–Rh–S(1)	174.33(5)
P(5)–Rh–S(2)	99.41(5)	S(1)–Rh–S(2)	77.94(5)
Pt(1)–S(1)–Pt(2)	89.97(4)	Pt(1)–S(1)–Rh	81.59(5)
Pt(2)–S(1)–Rh	81.90(4)	Pt(1)–S(2)–Pt(2)	89.00(4)
Pt(1)–S(2)–Rh	80.17(4)	Pt(2)–S(2)–Rh	81.36(4)

Table 2 (continued)

(d) $[IrPt_2(CO)(PPh_3)_5(\mu_3\text{-}S)_2]PF_6\cdot\frac{1}{2}CH_2Cl_2$, ***5b***			
Pt(1)–P(1)	2.284(2)	Pt(1)–P(2)	2.296(2)
Pt(1)–S(1)	2.359(2)	Pt(1)–S(2)	2.362(2)
Pt(2)–P(3)	2.280(2)	Pt(2)–P(4)	2.287(2)
Pt(2)–S(1)	2.338(2)	Pt(2)–P(5)	2.261(2)
Ir(1)–S(1)	2.363(2)	Ir(1)–S(2)	2.387(2)
C(91)–O(91)	1.059(10)		
Pt(1)···Ir(1)	3.1027(4)	Pt(2)···Ir(1)	3.0816(3)
Pt(1)···Pt(2)	3.315(5)		
P(1)–Pt(1)–P(2)	98.88(7)	P(1)–Pt(1)–S(1)	173.12(6)
P(1)–Pt(1)–S(2)	95.64(6)	P(2)–Pt(1)–S(1)	86.57(6)
P(2)–Pt(1)–S(2)	165.02(6)	S(1)–Pt(1)–S(2)	78.68(6)
P(3)–Pt(2)–P(4)	99.94(7)	P(3)–Pt(2)–S(1)	91.63(6)
P(3)–Pt(2)–S(2)	168.75(6)	P(4)–Pt(2)–S(1)	168.36(6)
P(4)–Pt(2)–S(2)	89.98(6)	S(1)–Pt(2)–S(2)	78.63(6)
C(91)–Ir(1)–P(5)	90.5(2)	C(91)–Ir(1)–S(1)	92.7(2)
C(91)–Ir(1)–S(2)	170.2(2)	P(5)–Ir(1)–S(1)	174.53(6)
P(5)–Ir(1)–S(2)	98.92(6)	S(1)–Ir(1)–S(2)	78.10(6)
Pt(1)–S(1)–Pt(2)	89.80(6)	Pt(1)–S(1)–Ir(1)	82.16(5)
Pt(2)–S(1)–Ir(1)	81.92(5)	Pt(1)–S(2)–Pt(2)	88.59(5)
Pt(1)–S(2)–Ir(1)	81.60(5)	Pt(2)–S(2)–Ir(1)	80.45(5)

[a] M(1) = 0.8Pt + 0.2Pd, M(2) = 0.6Pd + 0.4Pt, and M(3) = 0.7Pt + 0.3Pd.

$C_{90}H_{75}F_6ClP_6Pt_3S_2$: C, 50.5; H, 3.5; Cl, 1.7; P, 8.7; Pt, 27.4; S, 3.0%. Found: C, 50.0; H, 3.6; Cl, 2.1; P, 8.2; Pt, 25.5; S, 3.2%. $^{31}P\{^1H\}$-NMR ($CDCl_3$): δ 14.8 ppm (2P, t, ^1J(P–Pt) 3215 Hz), 12.9 ppm (2P, t, ^1J(P–Pt) 3210 Hz), and 8.9 ppm (1P, t, ^1J(P–Pt) 3819 Hz). IR (cm^{-1}) 839 vs (PF_6^-).

3.4. Synthesis of $[Pt_2Rh(CO)(PPh_3)_5(\mu_3\text{-}S)_2]PF_6\cdot CH_2Cl_2$, *4b*

A suspension of complex **1** (0.15 g, 0.1 mmol) and $RhClCO(PPh_3)_2$ (0.069 g, 0.1 mmol) in MeOH (40 cm^3) was flushed with CO and stirred in an autoclave for 24 h at 65°C under a CO pressure of 80 psi. The resultant clear yellow solution was concentrated to ca. 15 cm^3 under vacuum. The product was purified by a metathesis reaction with NH_4PF_6 to yield **4b** (Yield: 0.075 g, 34%). The product was recrystallized from CH_2Cl_2/hexane to give yellow crystals of **4b**. Using other Rh precursors such as $RhCl_3$, $RhCl(PPh_3)_3$ or $RhHCO(PPh_3)_3$ led to the same product. Anal. Calc. for $C_{92}H_{77}Cl_2F_6OP_6Pt_2RhS_2$: C, 54.2; H, 3.6; S, 3.0; P, 8.8%. Found: C, 53.0; H, 3.7; S, 3.0; P, 8.0%. $^{31}P\{^1H\}$-NMR ($CDCl_3$): δ 18.38 ppm (2P, ^1J(P–Pt) 3177 Hz), δ 15.78 ppm (2P, ^1J(P–Pt) 3162 Hz), δ_{Rh} 32.0 ppm [1P, d, ^1J(P–Rh) 169 Hz). IR (cm^{-1}) 1968 vs (CO), 841 vs (PF_6^-).

3.5. Synthesis of $[IrPt_2(CO)(PPh_3)_5(\mu_3\text{-}S)_2]PF_6\cdot\frac{1}{2}CH_2Cl_2$, *5b*

Complex **5b** was synthesized in a manner analogous to the **4b** by using **1** (0.15 g, 0.1 mmol) and $IrHCO(PPh_3)_3$ (0.101 g, 0.1 mmol) in MeOH (40 cm^3). The suspension was flushed with CO and stirred in an autoclave for 24 h at 65°C under a CO pressure of 80 psi. The resultant clear yellow solution was concentrated to ca 15 cm^3 under vacuum. The product was purified by a metathesis reaction with NH_4PF_6 to yield **5b**. (Yield: 0.079 g, 33%) The product was recrystallized from CH_2Cl_2/hexane to give yellow crystals of **5b**. Anal. Calc. for $C_{91.50}H_{76}ClF_6OP_6Pt_2IrS_2$: C, 50.5; H, 3.5; S, 2.9; P, 8.6%. Found: C, 49.5; H, 3.6; S, 3.2; P, 8.0%. $^{31}P\{^1H\}$-NMR ($CDCl_3$): δ 15.2 ppm (2P, ^1J(P–Pt) 3273 Hz), δ 11.9 ppm (2P, ^1J(P–Pt) 3216 Hz), δ 15.8 ppm. IR (cm^{-1}) 1954 vs(CO), 841 vs (PF_6^-).

3.6. X-ray crystallography

Single crystals of **2** and **3b** suitable for X-ray diffraction studies were grown from CH_2Cl_2/MeOH (1:1) by slow evaporation at r.t. in air, while single crystals of **4b** and **5b** were grown by slow diffusion of hexane into CH_2Cl_2 solution of the samples. The crystals of **4b** and **5b** are unstable (with respect to loss of solvent) upon isolation. Crystals **4b** and **5b** were hence sealed in a quartz capillary with the mother liquor during data collection. Data collection of **2, 4b** and **5b** were carried out on a Siemens CCD SMART system while a Siemen R3m/v diffractometer was used for **3b**. Details of crystal and data collection parameters are summarized in Table 1.

The structure of all the four complexes were solved by direct methods and difference Fourier maps. Full-matrix least-squares refinements were carried out with anisotropic temperature factor for all non-hydrogen

atoms. Hydrogen atoms were placed on calculated positions (C–H 0.96 Å) and assigned isotropic thermal parameters riding on their parent atoms. Initial calculations were carried out on a PC using SHELXTL PC software package; SHELXTL-93 [23] was used for the final refinement. Absorption correction was carried out by Sadabs. In **3b**, the three highest positive residues are located at 1.21, 0.84 and 0.55 Å from Pt(3), Pt(1) and Pt(2), respectively. The minimum residue is 0.46 Å from Pt(3) but on the opposite side of the maximum residue.

4. Supplementary materials available

Listing of detailed crystallographic data, refined atomic coordinates and isotropic thermal parameters, anisotropic thermal parameters, bond lengths and angles.

Acknowledgements

The authors acknowledge the National University of Singapore (NUS) (RP 960673) for financial support. Z.L. and H.L. thank NUS for scholarship award. Technical support from the Department of Chemistry of NUS is appreciated.

References

[1] W. Bos, J.J. Bour, P.P. Schlebos, J.P. Hageman, W.P. Bosman, J.M.M. Smits, J.A.C. Wietmarschen, P.T. Beurskens, Inorg. Chim. Acta 119 (1986) 141.
[2] H. Liu, A.L. Tan, Y. Xu, K.F. Mok, T.S.A. Hor, Polyhedron 16 (1997) 377.
[3] H. Liu, A.L. Tan, K.F. Mok, T.S.A. Hor, J. Chem. Soc. Dalton Trans. (1996) 4023.
[4] H. Liu, A.L. Tan, C.R. Cheng, K.F. Mok, T.S.A. Hor, Inorg. Chem. 36 (1997) 2916.
[5] C.E. Briant, D.L. Gilmour, M.A. Luke, D.M.P. Mingos, J. Chem. Soc., Dalton Trans. (1985) 851. (b) D.L. Gilmour, M.A. Luke, D.M.P. Mingos, J. Chem. Soc., Dalton Trans. (1987) 335.
[6] B.H. Aw, K.K. Looh, H.S.O. Chan, K.L. Tan, T.S.A. Hor, J. Chem. Soc., Dalton Trans. (1994) 3177.
[7] C.E. Briant, T.S.A. Hor, N.D. Howells, D.M.P. Mingos, J. Chem. Soc., Chem. Commun. (1983) 1118.
[8] C.E. Briant, T.S.A. Hor, N.D. Howells, D.M.P. Mingos, J. Organomet. Chem. 256 (1983) 15.
[9] T.S.A. Hor, J. Cluster Sci. 7 (1996) 263.
[10] F. Richter, H. Vahrenkamp, Angew. Chem. Int. Ed. Eng. 17 (1978) 444.
[11] R.D. Adams, T.S.A. Hor, Inorg. Chem. 23 (1984) 4723.
[12] R.D. Adams, M.P. Pompeo, W. Wu, Inorg. Chem. 30 (1991) 2899.
[13] S. Kuwata, Y. Mizobe, M. Hidai, J. Am. Chem. Soc. 115 (1993) 8499.
[14] H. Liu, A.L. Tan, K.F. Mok, T.C.W. Mak, A.S. Bastsanov, J.A.K. Howard, T.S.A. Hor, J. Am. Chem. Soc. 119 (1997) 11006.
[15] J.S.L. Yeo, G.M. Li, S.Y. Wong, W.-H. Yip, W. Henderson, T.C.W. Mak, T.S.A. Hor, J. Chem. Soc. Dalton Trans. (submitted).
[16] M.J. Pilkington, A.M.Z. Slawin, D.J. Williams, J.D. Woollins, J. Chem. Soc., Dalton Trans. (1992) 2425.
[17] A. Fumagalli, S. Martinengo, D. Galli, A. Albinati, F. Ganazzoli, Inorg. Chem. 28 (1989) 2476.
[18] A. Fumagalli, R.D. Pergola, F. Bonacina, L. Garlaschelli, M. Moret, A. Sironi, J. Am. Chem. Soc. 111 (1989) 165.
[19] C.H. Chin, T.S.A. Hor, J. Organomet. Chem. 509 (1996) 101.
[20] R. Ugo, G. La Monica, S. Cenini, A. Segre, F. Conti, J. Chem. Soc. A (1971) 522.
[21] J.A. Osborn, F.H. Jardine, J.F. Young, G. Wilkinson, J. Chem. Soc. (1966) 1711.
[22] D. Evans, G. Yagupsky, G. Wilkinson, J. Chem. Soc. A (1968) 2660.
[23] G.M. Sheldrick, SHELXTL-93 Program for Crystal Structure Refinement, University of Gottingen, Germany, 1993.